ELSEVIER

Nuclear Instruments and Methods in Physics Research A 485 (2002) 720–738

NUCLEAR INSTRUMENTS & METHODS IN PHYSICS RESEARCH Section A

www.elsevier.com/locate/nima

An algorithm for track reconstruction in the large angle spectrometer of the COMPASS experiment

K. Kurek[a,*,1], A. Korzenev[b], K. Kowalik[a,1], A. Mielech[a,1], E. Rondio[a,1], R. Windmolders[c,2]

[a] *Soltan Institute for Nuclear Studies, ul. Hoza 69, PL 00681 Warsaw, Poland*
[b] *Joint Institute for Nuclear Research, Dubna, Russia*
[c] *Physikalisches Institut Universität Bonn, Nussallee 12, D-53115 Bonn, Germany*

Received 25 June 2001; received in revised form 12 October 2001; accepted 16 October 2001

Abstract

An algorithm is presented for track reconstruction in the large angle spectrometer of a high energy fixed target experiment. Pattern recognition is provided by the association of segments found on both sides of the deflecting magnet within a variable roadwidth tuned to the characteristics of the experimental layout. Curved tracks swept away by the magnet are also searched for in the upstream telescope. The procedure has been tested on various sets of simulated data from the COMPASS experiment at CERN. The obtained track reconstruction efficiency reaches 85% for momenta above 2.5 GeV and is about 50% at 1 GeV, fulfilling one of the basic requirements of this experiment for the analysis of charmed meson decays.

PACS: 29.30.Aj; 29.40.Gx

Keywords: Charged particle spectrometer; Pattern recognition

1. Introduction

Our knowledge of the polarized parton distribution functions (pPDF) has been much improved by the experiments in polarized deep inelastic scattering performed over the last 10 years with the exception of the gluon spin distribution (ΔG) which remains poorly constrained as well in magnitude as in shape. A more precise evaluation of ΔG can be obtained from asymmetry measurements in specific semi-inclusive μ–N interactions which are dominated by the photon–gluon fusion process (''PGF'') and therefore are specially sensitive to the gluon spin. This is the case for charmed meson production which can be most conveniently detected by the 2-body decays $D^0 \to K^-\pi^+$ and $\bar{D}^0 \to K^+\pi^-$. In addition, the separation of these decays from the background $K\pi$ mass distribution can be greatly improved for those resulting from D^* decays: $D^* \to D\pi$ (about $\frac{1}{3}$

*Corresponding author. Tel.: +48-22-553-22-39; fax: +48-22-621-28-04.

E-mail address: krzysztof.kurek@fuw.edu.pl (K. Kurek).

[1] This work was supported in part by KBN SPUB Nr 621/E-78/SPUB-M/CERN/P-03/DZ298/2000-2002 and Grant No. 2 P03B 113 19.

[2] Supported by the Bundesministerium für Bildung und Forschung, Contract No. 06BN908I.

0168-9002/02/$ - see front matter
PII: S0168-9002(01)02123-4

of the total sample) if the additional π is also detected. In its muon program the COMPASS experiment, presently under construction at CERN, aims at a precise determination of the gluon polarization from measurements of those charmed meson decays [1].

The incoming muon energy will be chosen in the range 100–200 GeV in order to maximize the incoming flux and the charm particle production rate. Muons will interact with the target material (^{6}LiD or NH_3) contained in two 60 cm long cells located in a 2.5 T magnetic field produced by a 3 m long superconducting solenoid. The two cells, separated by an interval of 10 cm, will be polarized by dynamic nuclear polarization (DNP) [2] in opposite directions along the beam axis. Secondary particles within the 180 mrad magnet aperture will be detected in a two stage spectrometer. The magnet in the first part (the Large Angle Spectrometer — LAS), located 3.5 m downstream the target center, has a bending power of 1 T m and a large acceptance for all secondary particles with momentum as low as 0.3 GeV. The magnet of the second spectrometer is located 14 m further downstream and is tuned to bend the beam particles by about 10 mrad. Its acceptance for secondary particles starts around 2 GeV and reaches its plateau value at about 5 GeV.

Simulation studies of D^0 and D^* production by "quasi-real" virtual photons ($Q^2 \simeq 0$) have been performed using the heavy-flavor event generator AROMA [3]. The momentum and production angle distributions of the decay kaons and pions are shown in Fig. 1 for an incoming muon energy of 100 GeV. The average momenta of the kaons and pions from D^0 2-body decays are of the order of 10 GeV and their average polar angles of about 100 and 150 mrad, respectively, while the pion from D^* decay has an average momentum of 1.6 GeV and an average angle of 50 mrad. These values show that the LAS will play a crucial role in the reconstruction of charmed meson decays and set the boundary requirements for the detection of low momentum tracks.

Track finding in the COMPASS LAS is complicated by the absence of field-free regions. For this reason, pattern recognition based on the search of straight segments according to standard criteria would be strongly biased against low momentum tracks and thus unacceptable in view of the physics aims of COMPASS. On the other hand, due to the high occupancy in the central part of the spectrometer, methods based on the association of space points reconstructed in the various detector stations would lead to an excessive demand of CPU time. Several track finding algorithms adapted to the COMPASS requirements have been developed. In the one described in this paper, the search of lines on both sides of the first bending magnet (SM1) is performed iteratively with rejection criteria readjusted at each turn and with the option to restrict the search to well-defined groups of detectors. Combinatorial ambiguities are further reduced by requiring that the reconstructed tracks originate from the target cells.[3] This procedure has been optimized for the COMPASS running conditions and extensively tested with simulated events. Special emphasis has been put on the reconstruction of low momentum tracks ($0.5 \leqslant p \leqslant 5.0$ GeV) which can only be detected in the LAS.

The next two sections will describe the various detectors of the LAS and the characteristics of the field map of its bending magnet. In the following ones we will discuss the various steps of the track finding algorithm and the practical aspects of its implementation. The last section will present the expected reconstruction efficiency as determined from simulated data.

2. The COMPASS large angle spectrometer layout

The COMPASS experiment plans to run at a beam intensity as large as 10^8 muons/s. The necessity to cope with the resulting high particle rates has led to the use of hybrid detector stations, the central part of the spectrometer being covered by small detectors which can handle high rates, while the outer part is covered by large drift detectors [4].

Between the target and SM1, particles will be detected in several planes of scintillating fibers if

[3] This condition can be modified in order to search for tracks originating from neutral particle decays.

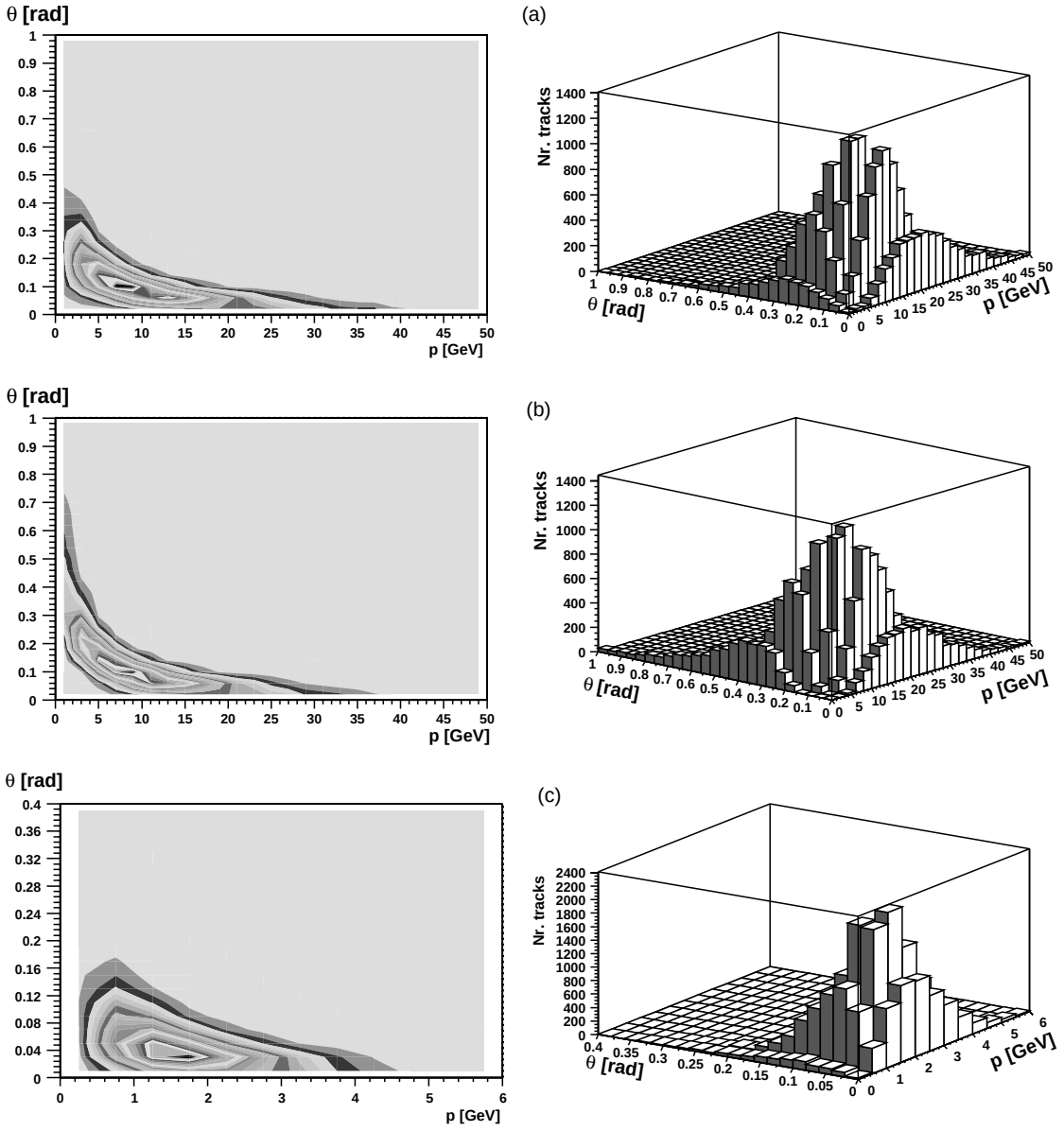

Fig. 1. Angle and momentum distribution for kaons from D^0 decay (a), pions from D^0 decay (b) and pions from D^* decay (c) at 100 GeV incident momentum.

they are very close to the beam axis, in 3 Micromegas [5] if they are at a distance between 5 and 40 cm with respect to the beam axis and in two drift chambers if they are further away.

Behind SM1, particles pass through GEM [6], straw detectors or scintillating fibers before entering the RICH counter used for particle identification [7]. A general view of the LAS is shown in Fig. 2. The reference frame is a right handed coordinate system, centered at the middle of the target with its Z-axis along the beam line and its Y-axis pointing upward.

After crossing the RICH, particles staying close enough to the beam axis are further detected in

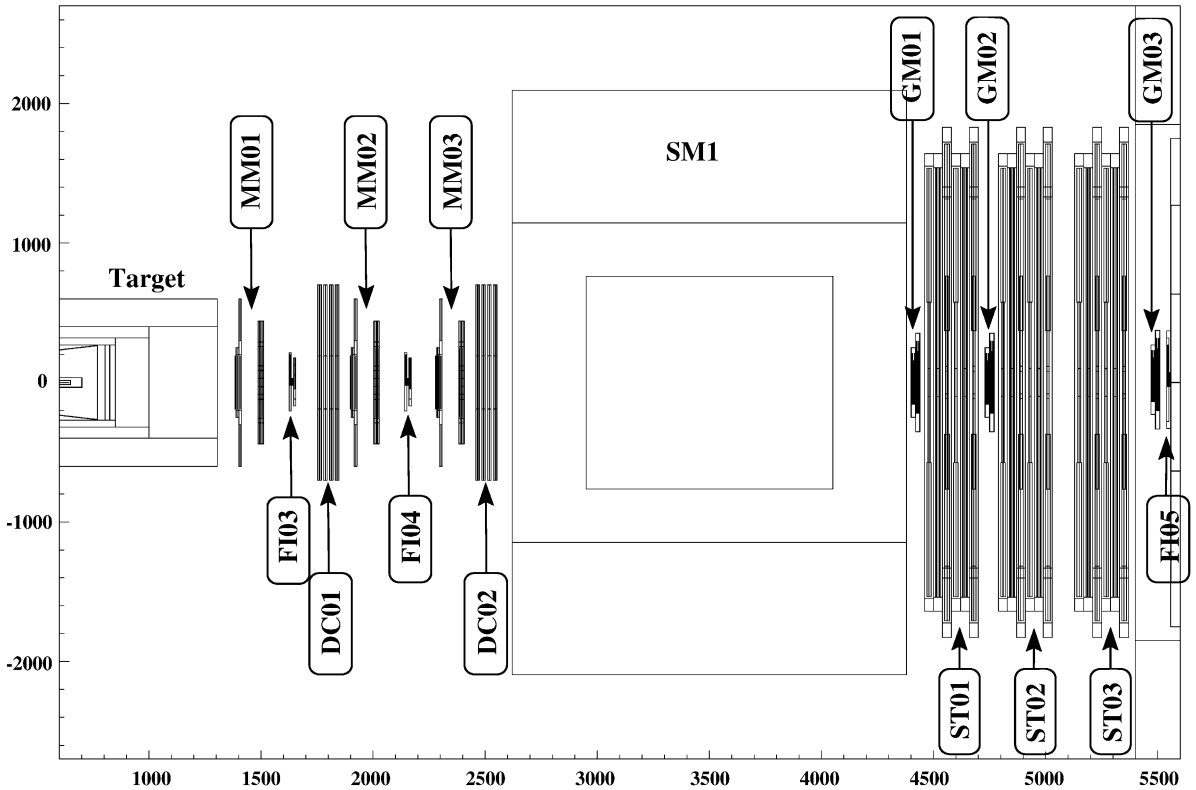

Fig. 2. An overview of the LAS in the horizontal plane. The scales on the axes are in mm.

several scintillating fiber, GEM or MWPC stations which do not belong to the LAS but will be used for track extrapolation (Section 4.3). The geometrical characteristics and the position of all detectors are listed in Table 1 where the plane orientation defines the measured coordinate ($x(\theta = 0), y$ or θ).

3. The field map of the large aperture magnet SM1

The SM1 magnet is a dipole with a pair of bedstead coils placed at 3.5 m from the target center. The strength of the field, the main component of which goes from top to bottom, can be varied by changing the height of the central gap. In the COMPASS muon program the largest gap size (1.32 m at the entrance) will be used. Fig. 3 shows a sketch of the magnet in this configuration. Yoke pieces have been introduced to satisfy the requirement of orthogonality of field lines and particle trajectories. The internal surface of these pieces has been designed to fit a cone with its top at the position of the target center so that field lines are orthogonal to the lines originating from the target center.

Field measurements have been performed with a sensor consisting of four Hall detector cubes of $15 \times 15 \times 15\ \text{mm}^3$. The Hall plates are mounted on each of the six sides of the cube. Each pair of plates installed on opposite sides measures one of the field components. All three components were measured simultaneously and the field in the center of the cube could be obtained by averaging the values of each pair of plates. This method thus provides the values of field components at the same spatial point without any interpolation.

The field map of SM1 has been obtained from the measured values with small corrections taking into account the non-orthogonality of the Hall

Table 1
Detectors in the COMPASS LAS and detectors used for track extrapolation

Name	Type	Size (mm × mm)	First and last plane position along beam (mm)	Nr. of planes	Plane orientation	Dead region (mm)
MM01	Micromegas	380×380	1390–1510	4	$x\ y\ 20^\circ\ -20^\circ$	$\varnothing = 50$
FI03	Scint. fibers	50×50	1630–1650	3	$x\ y\ 45^\circ$	—
DC01	Drift chamb.	1400×1240	1760–1840	8	$2x\ 2y\ 2\times 20^\circ\ 2\times(-20^\circ)$	$\varnothing = 380$
MM02	Micromegas	380×380	1910–2020	4	$x\ y\ 20^\circ - 20^\circ$	$\varnothing = 50$
FI04	Scint. fibers	50×50	2140–2160	3	$x\ y\ 45^\circ$	—
MM03	Micromegas	380×380	2290–2400	4	$x\ y\ 20^\circ - 20^\circ$	$\varnothing = 50$
DC02	Drift chamb.	1400×1240	2460–2550	8	$2x\ 2y\ 2\times 20^\circ\ 2\times(-20^\circ)$	$\varnothing = 380$
GM01	Gem	310×310	4410–4430	4	$x\ y\ 45^\circ - 45^\circ$	$\varnothing = 50$
ST01	Straws	3080×2260	4480–4680	12	$2x\ 2y\ 2\times 10^\circ$ $2x\ 2y\ 2\times(-10^\circ)$	200×200
GM02	Gem	310×310	4740–4760	4	$x\ y\ 45^\circ - 45^\circ$	$\varnothing = 50$
ST02	Straws	3080×2260	4810–5010	12	$2x\ 2y\ 2\times 10^\circ$ $2x\ 2y\ 2\times(-10^\circ)$	200×200
ST03	Straws	3080×2260	5150–5350	12	$2x\ 2y\ 2\times 10^\circ$ $2x\ 2y\ 2\times(-10^\circ)$	200×200
GM03	Gem	310×310	5480–5500	4	$x\ y\ 45^\circ - 45^\circ$	$\varnothing = 50$
FI05	Scint. fibers	80×80	5540–5550	2	$x\ y$	—
GM04	Gem	310×310	9110–9130	4	$x\ y\ 45^\circ - 45^\circ$	$\varnothing = 50$
PS01	Prop. chamb.	1520×1200	9230–9270	4	$-10^\circ\ x\ 10^\circ y$	$\varnothing = 120$
GM05	Gem	310×310	13 000–13 010	4	$x\ y\ 45^\circ - 45^\circ$	$\varnothing = 50$
FI06	Scint. fibers	80×80	13 020–13 070	2	$x\ y$	—
PA01	Prop. chamb.	1520×1200	13 180–13 220	3	$10^\circ\ x - 10^\circ$	$\varnothing = 170$
PA02	Prop. chamb.	1520×1200	14 980–15 010	3	$10^\circ\ x - 10^\circ$	$\varnothing = 170$
GM06	Gem	310×310	15 150–15 170	4	$x\ y\ 45^\circ\ -45^\circ$	$\varnothing = 50$

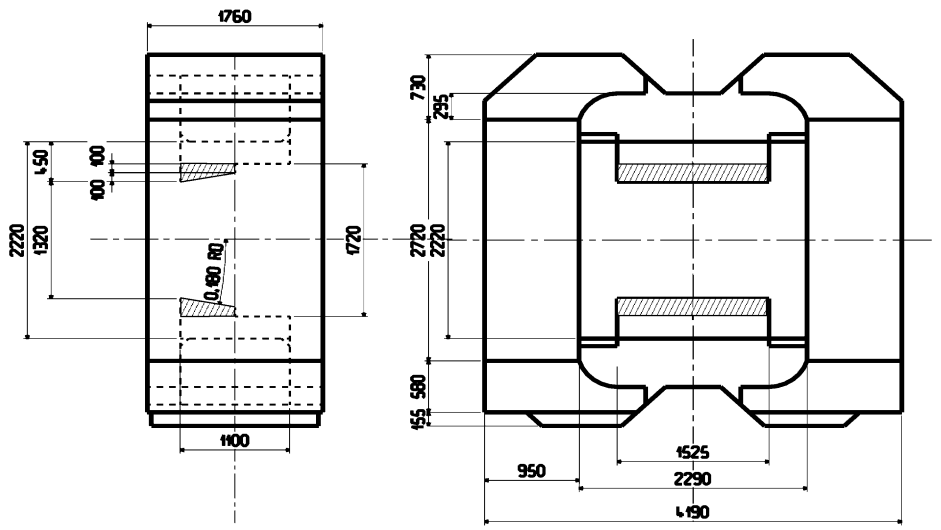

Fig. 3. Sketch of the SM1 magnet seen from side (left) and along the beam direction (right). The shaded areas correspond to the yoke pieces (see text). Coordinates are given in mm.

plates, the planar Hall effect and the misalignment of the sensor with respect to the SM1 coordinate system. In addition, symmetry conditions based on the symmetry in the magnet construction have been imposed.[4] The main field component B_y is assumed to be symmetric with respect to the $y = 0$ plane while B_x, B_z are assumed to be antisymmetric and thus to vanish for $y = 0$.

The main component (B_y), plotted along the beam axis OZ, shows a strongly asymmetric shape with respect to the median plane of the magnet, which becomes more and more pronounced when moving away from the $y = 0$ plane (Fig. 4). This pattern remains almost unchanged over a wide range of $x(-0.6 \leqslant x \leqslant 0.6$ m). At a distance of 1 m from the center (i.e. well outside the magnet poles), the value of B_y remains quite large ($\simeq -(0.18 - 0.25)$ T) with little variation for $-0.6 \leqslant x, y \leqslant 0.6$ m.

The field integral of $B_y(z)$ measured along the beam axis starting from the first detector plane behind the target is shown in Fig. 5. The full integral (-1 T m) corresponds to a deflection of 300 mrad at a momentum of 1 GeV. It can be noticed that for a particle following the beam axis 15% of the integral are already reached before the second drift chamber DC02 while the last 15% are applied after the first straw station ST01. For particles with momenta of the order of 1 GeV, the deflection in the upstream part of the LAS is thus sufficient to allow a significant evaluation of the track parameters. This feature plays an important role in the reconstruction algorithm described in this paper: track reconstruction is generally based on the association of "nearly straight" segments found in the telescopes before and behind SM1 but the momentum of slow particles which are no longer detectable behind SM1 can also be evaluated from the hits found in the upstream telescope, taking into account the bending due to the SM1 fringe field.

The superconducting target solenoid is presently under construction and its field map has been calculated according to the specifications provided by the manufacturers. The field component along the beam axis is still of the order of 1 T at the position of the most upstream detectors and its effect is still sizeable at the position of the second drift chamber DC02. This is best seen in the smaller field components B_x and B_z. The lines (Fig. 6a) presenting the values of B_x measured along the vertical axis OY for different values of x all intersect at the point ($B_x = 0, y \simeq -0.10$ m) while the symmetry properties of SM1 would require the intersection to be at $y = 0$ in the

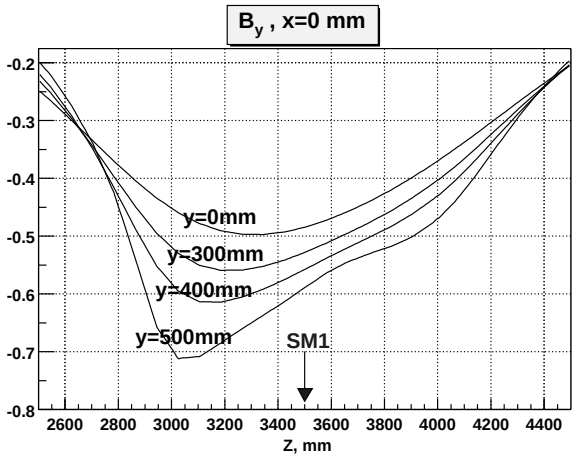

Fig. 4. Main component of the magnetic field (in T) as a function of the position along the beam direction. The arrow shows the position of the median plane of SM1. The curves correspond to different heights.

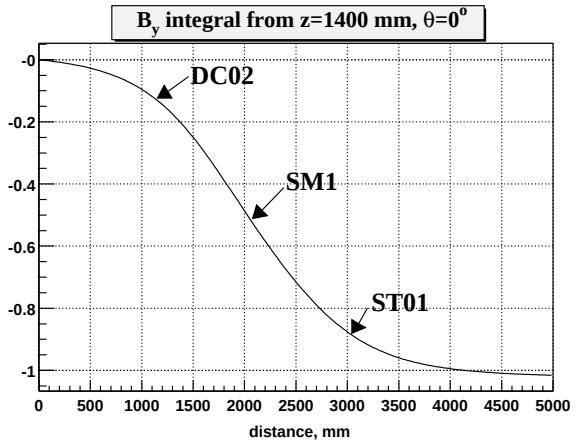

Fig. 5. Value of the field integral (in T m) along the beam axis from the first detector plane to the current Z position.

[4] This symmetry is not perfect because the construction of SM1 is not absolutely symmetric.

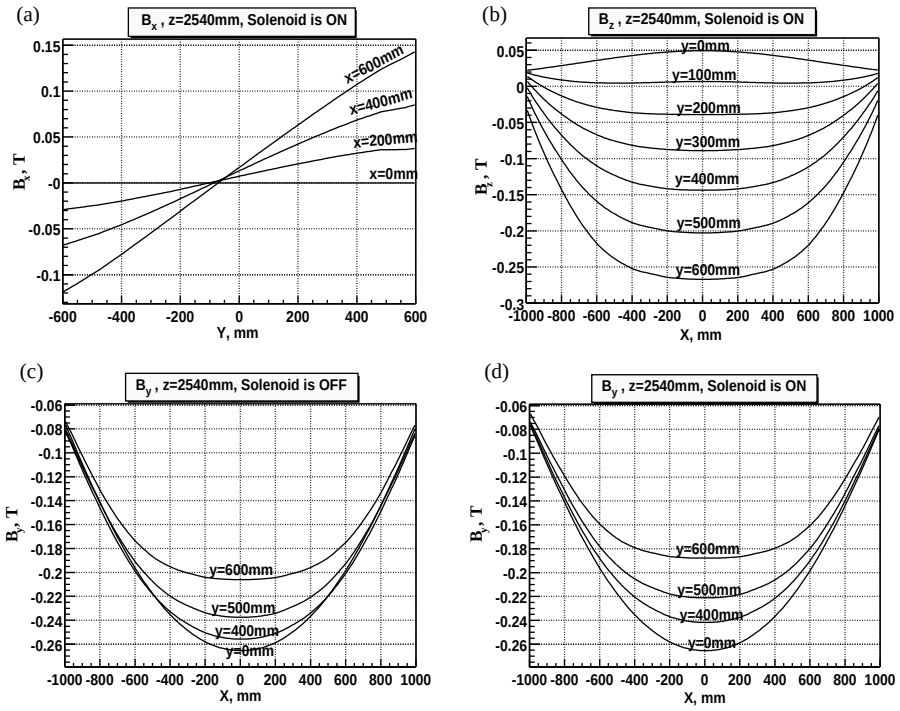

Fig. 6. Some characteristics of the SM1 field at the position of DC02: variation of B_x along the vertical axis for various x values (a); the B_z component as a function of x (b); the main component B_y as a function of x with solenoid field off (c) and on (d). Coordinates are given in mm, fields in T.

absence of other contributions to the field. The plot of B_z (Fig. 6b) as a function of x also shows non-zero values for $y = 0$ which are entirely due to the fringe field of the target solenoid.

The effect of the solenoid on the main field component of SM1 is shown in Fig. 6c and d. The variation of B_y is negligible at $y = 0$ but reaches about 10% at a distance of 0.5 m from the $y = 0$ plane.

From these plots, it can be concluded that the parametrization of particle trajectories in the upstream telescope of the LAS will require the evaluation of the target solenoid field and of the SM1 field at many points. Trajectories are expected to deviate significantly from straight lines for low momentum particles. The bending is mainly in the horizontal plane ($y = 0$) but effects due to the x component of the field become non-negligible for particles at large enough distance from the beam axis. An overview of the field configuration $|B|$ over the full LAS is shown in Fig. 7. This complicated pattern rules out the use of simple analytic models of trajectories and justifies the use of a dedicated track reconstruction algorithm.

4. The track reconstruction algorithm

The algorithm described in this paper basically follows a *projection method* where track candidates are first searched for separately in the horizontal (XZ) and vertical (YZ) planes and, at the next stage, associated in space by making use of the inclined detector planes. This method is used in a similar way for the search of so-called "lines" in the telescopes before and behind SM1. The candidates found on both sides of SM1, which are often much more numerous than the number of real tracks, are tested for compatibility in a procedure involving a spline fit before they are registered as "tracks".

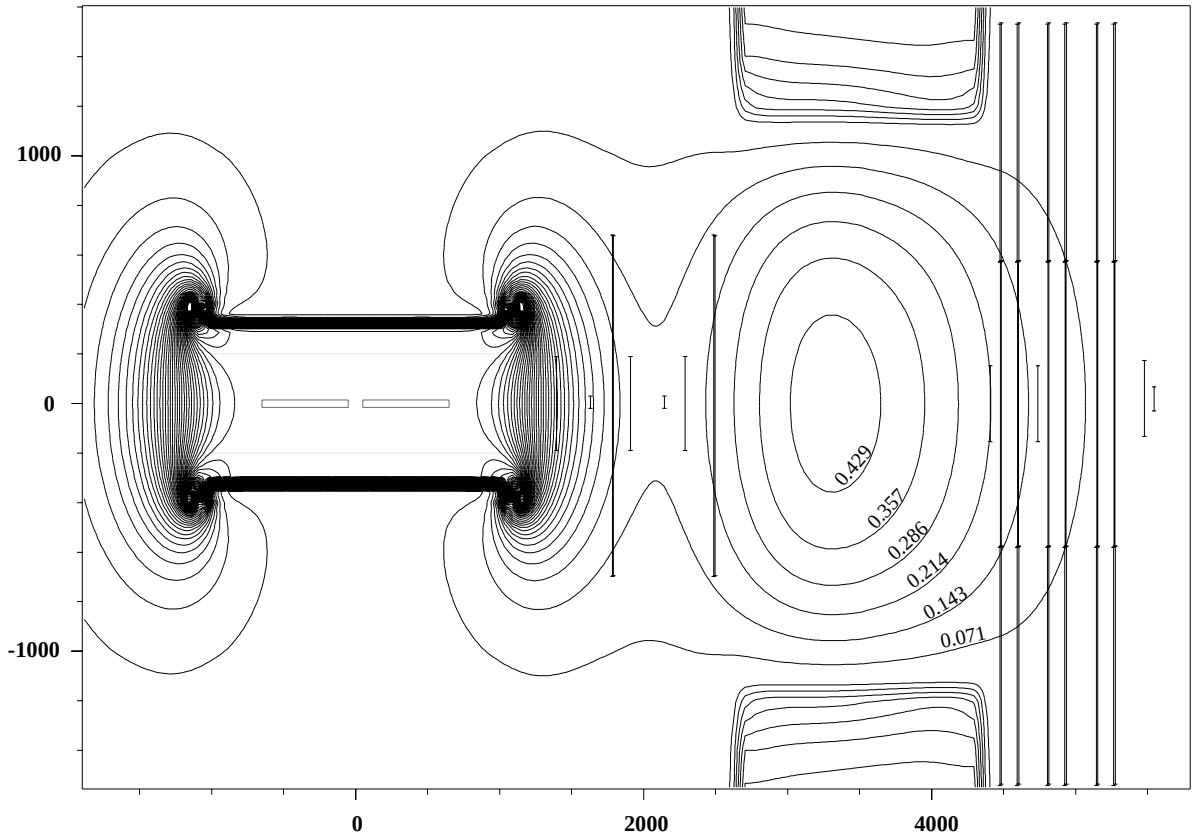

Fig. 7. An overview of the LAS with "equipotential lines" of the magnetic field $\sqrt{B_x^2 + B_y^2 + B_z^2}$ (in T). The scales on the axes are in mm.

At the end of the process the procedure provides the list of hits assigned to each track as well as estimates of the track parameters at the first and last measured point. This information is transferred to the global data reconstruction program where it is merged with results from the reconstruction in the forward spectrometer.

4.1. Search for lines upstream or downstream SM1

The present algorithm uses "hits" found in various detector planes and tries to associate them in order to form "lines". These hits are obtained from the collected signals converted into coordinates according to the detector description. A line candidate is initially defined by two orthogonal projections, each of them defined by a pair of hits. One pair of hits thus provides the x coordinate and the slope $\mathrm{d}x/\mathrm{d}z$ and the other pair provides the y coordinate and the slope $\mathrm{d}y/\mathrm{d}z$. These four hits belong to two pairs of orthogonal detector planes, the so-called "reference planes". Since the reference planes forming a pair must be well separated to obtain a reasonable accuracy on the line direction, we require them to be located in the upsteam and downstream halves of the telescope. Each plane with the desired wire orientation is used in turn as reference plane, starting from the most external one. All pairs of hits in these planes are tried in order to define a XZ or YZ projection, except those which have been flagged because they already belong to an accepted line.

The selection of hits in the reference planes is thus always based on four independent loops but their ordering may vary in different cases, mainly for reasons of efficiency. For the search of lines

behind SM1, the most external loop is on the (non-bending) Y planes closest to the magnet and the most internal one on the (bending) X planes in the downstream half. In front of SM1, the ordering of loops may start either from the Y planes closest to the magnet or from the X planes closest to the target and is varied in turn from one iteration to the next. The ordering of loops may to some extent affect the result because the list of tested hit combinations is not exhaustive. The adopted choice was found to be the optimal one in order to maximize the reconstruction efficiency and to keep the fraction of faked tracks as low as possible.

In the non-bending YZ projection it is always checked that the segment (defined by a pair of selected hits) points to the target within a tolerance accounting for the residual curvature. The same test is also performed in the XZ projection for lines in front of SM1.

In the most confusing cases, when the hit multiplicity in one of the reference planes exceeds by far the average multiplicity, a shortened procedure is adopted. In this case, only hits in the outer loops on X and Y planes are tested systematically in association with the hit in the inner loop defining the segment pointing closest to the target center.

When the orthogonal projections have been defined by two pairs of hits compatible with the target pointing conditions, their association to a track in space has to be validated by the presence of hits in several "additional planes", including at least some inclined (θ) planes. The line defined by the four hits in the reference planes is extrapolated to all remaining planes and hits within a given road around the impact are selected. The validation requires a minimal number of planes with some selected hits. All combinations of such hits are tried in turn and the optimal one is selected on the basis of the lowest χ^2 in a straight line fit.[5]

A line is accepted when its χ^2 is below a predefined limit which takes into account the curvature of low momentum tracks. Hits associated to an accepted line are "flagged". These hits can no longer be used in reference planes to define new projections but are still available for the validation of other lines (this feature accounts for the fact that some hits may belong to more than one track).

When a line has been accepted, the three internal loops on reference planes are left while the most external one is being continued. This apparently arbitrary feature introduces some dependence on the ordering of plane loops but was found essential to avoid accumulating a large number of duplicated lines due to the redundant choice of reference planes. It implies that two tracks sharing a common hit in the first reference plane can never be found in the same loop. However, the second one can still be found with a different choice of reference planes and the reconstruction efficiency will be unaffected by this limitation.

4.2. Association of track segments before and behind SM1

Since SM1 mainly bends the tracks in the (XZ) plane, segments of a same track found on both sides of the magnet are expected to have about the same slope $\mathrm{d}y/\mathrm{d}z$ and to extrapolate to about the same y position in the median plane of the magnet. These simple association criteria are tested for all pairs of segments with predefined tolerances. Accepted pairs are further tested by a spline fit following closely the method described in Ref. [8]. The basic principles of this method are briefly presented below.

The measured pairs of coordinates (x_i, z_i) and (y_i, z_i) are first interpolated by a cubic spline in order to define a set of intermediate points at equally spaced positions between the first and the last detector plane. The slopes $(\mathrm{d}x/\mathrm{d}z)$ and $(\mathrm{d}y/\mathrm{d}z)$ and the components of the magnetic field B are evaluated at all measured and intermediate points in order to calculate the functions:

$$f_1(z) = k(z)(B_z\,\mathrm{d}y/\mathrm{d}z + B_x\,\mathrm{d}x/\mathrm{d}z\,\mathrm{d}y/\mathrm{d}z - B_y(1 + (\mathrm{d}x/\mathrm{d}z)^2)) \quad (1)$$

$$f_2(z) = k(z)(-B_z\,\mathrm{d}x/\mathrm{d}z - B_y\,\mathrm{d}x/\mathrm{d}z\,\mathrm{d}y/\mathrm{d}z + B_x(1 + (\mathrm{d}y/\mathrm{d}z)^2)), \quad (2)$$

[5] The combinatorial ambiguities may be further reduced by the correlated two-dimensional information provided by the GEM detector planes, which is not taken into account here.

with

$$k(z) = 0.3\sqrt{1 + (\mathrm{d}x/\mathrm{d}z)^2 + (\mathrm{d}y/\mathrm{d}z)^2}\ \mathrm{GeV/T\,m}. \tag{3}$$

The functions $f_1(z)$ and $f_2(z)$ are the products of the particle momentum p times the second derivatives $\mathrm{d}^2x/\mathrm{d}z^2$ and $\mathrm{d}^2y/\mathrm{d}z^2$ at a given z position along the trajectory. The evaluation of their double integrals $FD_1(z)$, $FD_2(z)$ by a quintic spline interpolation provides a set of relations between the track parameters and the measured coordinates t_k in all planes.

For a plane with orientation θ_k located at $z = z_k$ the predicted coordinate will be

$$\begin{aligned} v_k = {} & \sin\theta_k x_0 - \cos\theta_k y_0 + \sin\theta_k (z_k - z_0) x_0' \\ & - \cos\theta_k (z_k - z_0) y_0' + \frac{1}{p}(\sin\theta_k FD_1(z_k) \\ & - \cos\theta_k FD_2(z_k)) \end{aligned} \tag{4}$$

where the track parameters are the momentum p, the coordinates (x_0, y_0) and the slopes (x_0', y_0') at the reference point $z = z_0$. They are obtained in a least squares fit by minimizing

$$\chi^2 = (t_k - v_k)^{\mathrm{T}} (V^{-1})(t_k - v_k) \tag{5}$$

where V is the error matrix and the index k runs over all measurements.

If the only errors to be considered are those from the plane resolution (σ_k), the χ^2 reduces to a sum over all measurements:

$$\chi^2 = \sum (t_k - v_k)^2/\sigma_k^2 \tag{6}$$

and the optimal values of the parameters can be directly determined. In contrast, the errors due to multiple Coulomb scattering (MCS) depend on the particle momentum as well as on the amount of material it has crossed and can only be evaluated after a preliminary determination of the track parameters. The error matrix including the MCS contributions is non-diagonal and its inversion for testing each pair of segments would be by far too demanding in CPU time. For this reason MCS errors are only evaluated approximately using a set of error matrices defined for various intervals of $1/p$ and inverted at the initialisation stage. The χ^2 obtained from Eq. (5) is only approximate but is found to provide an efficient discrimination against false combinations of hits. For tracks exceeding the χ^2 limit by less than a factor 5 the following rescue procedure is applied: all hits giving contributions above a predefined limit are removed and the fit is redone. Tracks fulfilling the χ^2 criterion after this procedure are kept.

The results of this procedure are presented in the plots of Fig. 8. The first plot shows that the purity of accepted track candidates (i.e. the fraction of their hits belonging to a single generated track) is peaked at high values. For further comparisons between reconstructed and generated tracks as well as for efficiency calculations, we will consider a track as "correctly reconstructed" when the fraction of hits belonging to a single generated track is larger than 80%. Tracks not fulfilling this condition will be considered as "faked tracks". The second plot shows, for the tracks satisfying this criterion, the difference between generated and reconstructed momenta at the position of the first detector plane. The distribution is correctly centered and has an RMS of about 0.25 GeV for a range of ± 2 GeV. The third one shows that the generated and reconstructed values of the momentum are in good agreement over the full range of the distribution. The last plot shows the *pull*, i.e. the difference between generated and reconstructed values of $(1/p)$ divided by the assigned error. In order to test the error evaluation, the plot is restricted to tracks containing only orrect hits. The resulting distribution has the expected Gaussian shape with $\sigma \simeq 1.40$. The errors on the momenta thus appear to be correctly defined within a factor of 1.5, which is easily understood in view of the approximations mentioned above.

4.3. Extrapolation to the second spectrometer

Only detectors located between the target and the RICH have been used in the procedure described so far. Additional information exists for tracks observed in the detectors located behind the RICH (i.e. the third group of detectors listed in Table 1). This information is, however, limited to the track direction since there is no magnetic field in this region.

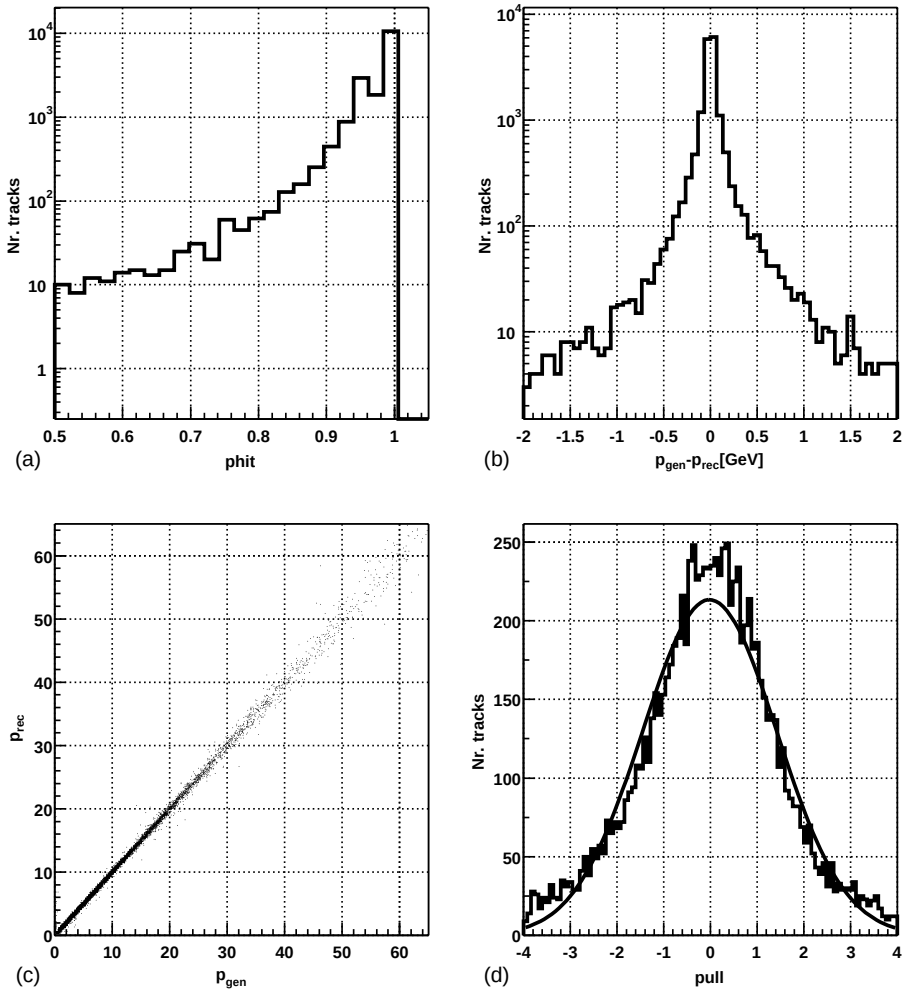

Fig. 8. Purity (p_{hit}) of selected track candidates (a), distributions of $p_{gen} - p_{rec}$ (b), plot of the reconstructed momentum p_{rec} versus the generated momentum p_{gen} (c), distribution of "pull" defined as $1/p_{gen} - 1/p_{rec}$ divided by its error (d). Plots (b) and (c) are for tracks with $p_{hit} \geqslant 0.80$, plot (d) for tracks containing only correctly assigned hits ($p_{hit} = 1.0$). The quoted momenta are evaluated at the position of the first detector plane.

The fitted track parameters are used to extrapolate the track behind the RICH and to search for additional hits. As a first step, hits close to the extrapolated track are looked for in the planes of GM04 and PS01 and a straight line fit is performed in the range extending from ST02 (to avoid distortions due to the residual field of SM1) up to $z = 10$ m. If a satisfactory result is obtained the track is further extrapolated to $z = 16$ m and a new straight line fit is performed including all detectors located between ST02 and the second spectrometer magnet.

It is observed that about half of the extrapolated tracks end after the first multi-wire chamber (PS01), while the others reach PA01. In both cases a significant effect is observed in the track fit: the accuracy in the determination of the slopes is improved by a factor of about 1.6 for dy/dz and by a factor in the range 1.6–3.0 for dx/dz, as a consequence of the extended lever arm. For tracks

entering the more precise central detectors (GM04-GM05-GM06), this factor may become as large as 10 for both slopes. In all cases, these extrapolations improve significantly the precision of the track parameters at the last measured point and are thus valuable for further processing involving the forward spectrometer.

4.4. Fringe field reconstruction

Large angle lines found in the first telescope and failing the association tests to any line of the second telescope may correspond to tracks which are out of the aperture of SM1 or to tracks which cross SM1 but are so strongly bent that there are too few hits to define a line behind the magnet. This happens for some low momentum tracks and affects the reconstruction efficiency for the procedure described so far. For this reason a rescue procedure for tracks observed only in the detectors upstream of SM1 has been implemented.

Track finding in the first telescope becomes specially difficult in the central region where the high occupancy makes the hit selection extremely ambiguous. Consequently the rescue procedure is restricted to track segments detected in DC02, i.e. away from the central region at the entrance of SM1. The search of these segments is performed according to the method described in Section 4.1, with the most external loop on the non-bending Y planes of DC02. The spline fit performed for these lines is similar to the one described above, with a reduced number of interpolation planes, and it provides an estimate of the particle momentum based on the curvature in the SM1 fringe field. When an acceptable fit is obtained, the track is added to those obtained in the normal procedure. The accepted track sample is increased by about 14% due to this rescue procedure.

In order to improve their accuracy, the accepted "fringe field tracks" are extrapolated across SM1 (according to the estimated momentum) and additional hits are looked for in GM01 and in ST01. In practice, the search area has to be quite large ($0.5 \times 0.3\ \mathrm{m}^2$), especially in the bending plane, since the poorly constrained momentum may lead to an inaccurate extrapolation. At least four hits in planes with different orientations are required. It is also checked that these four hits correspond to a space point located within a given distance of the extrapolated track and fulfilling the usual relations between position and slopes. The parameters of the tracks satisfying these criteria (about 20% of the sample) are redetermined in a new fit including the hits found behind SM1.

The results of track reconstruction in the fringe field of SM1 are shown in Fig. 9. In average the fringe field tracks are more contaminated by incorrect hits than those reconstructed in the normal procedure and the sample is thus expected to contain a larger fraction of faked tracks. The plot of reconstructed versus generated momenta shows a much larger dispersion than for normal reconstruction: the momentum resolution is degraded by a factor resulting from the respective values of the field integrals $\int B\,\mathrm{d}l$ (Fig. 5). For fringe field tracks also detected behind SM1 the momentum resolution is unchanged compared to the normal reconstruction.

5. Algorithm implementation

The algorithm described in the previous section has been tested and tuned to the needs of the COMPASS experiment. The goal was to reach high efficiency of track reconstruction, especially for particles at low momentum ($p \leqslant 5$ GeV), with a low fraction of faked tracks. The difficulties are due to the strong fringe field generated by SM1, the high density of hits in the central region of the detectors and the combination of detectors of different size and resolution in the LAS.

As input the algorithm uses all hits (converted to coordinates) collected in the detector planes of the LAS, except for the drift type detectors (DC's and ST's) where the left–right ambiguity is solved first. A simple procedure testing target pointing for each pair of hits in neighbouring planes with identical orientation allows us to apply the selection in about 85% of the cases and provides the correct answer in 90% of those [9]. Identified mirror hits are removed from the list of hits available for track reconstruction.

In the tuning of the algorithm, a compromise had to be found between the requirements

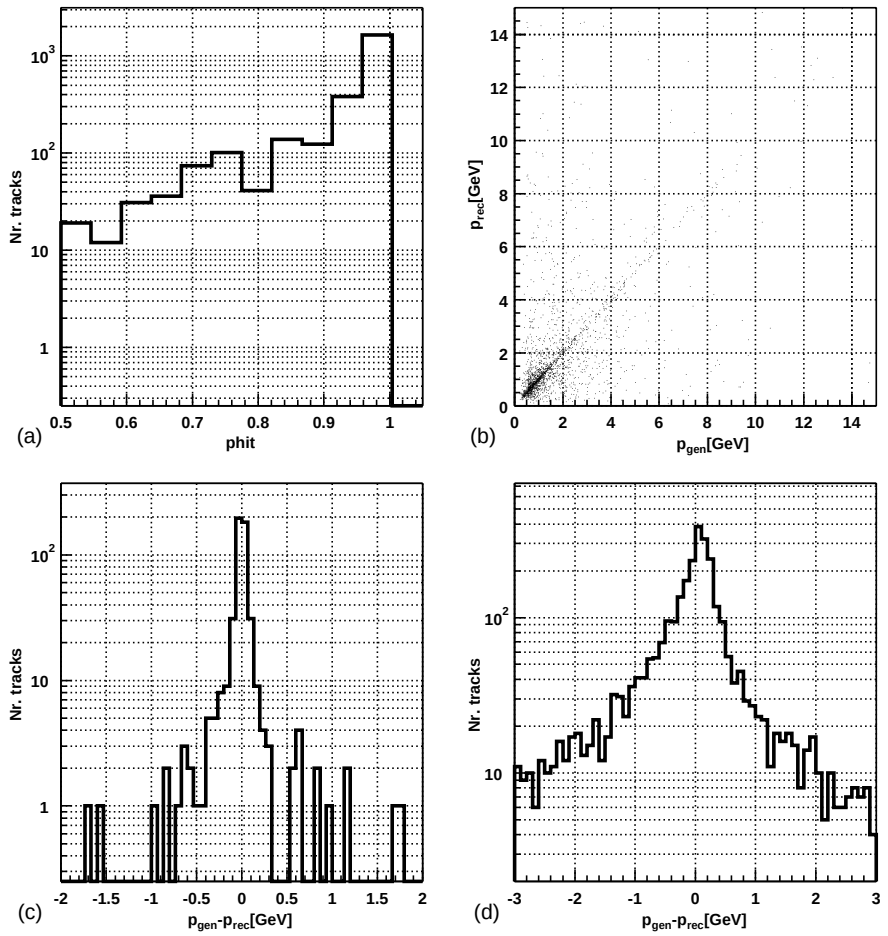

Fig. 9. Track reconstruction in the fringe field of SM1: purity (p_{hit}) of selected track candidates (a), plot of the reconstructed momentum p_{rec} versus generated momentum p_{gen} (b), distributions of $p_{\mathrm{gen}} - p_{\mathrm{rec}}$ for tracks also detected in the first detector planes behind SM1 (c), and for the other tracks reconstructed in the fringe field (d). Plots (b), (c) and (d) are for tracks with $p_{\mathrm{hit}} \geqslant 0.8$.

resulting from high reconstruction efficiency and small admixture of faked tracks. The former one leads to the use of very wide roads in the initial search of lines while the latter one imposes rather narrow roads. These contradictory requirements result from the fact that real tracks have some curvature due to the residual magnetic field while at the initial stage the procedure searches for straight segments in two projections. This problem is solved in the present algorithm by an iterative procedure. A search of tracks is first performed with road parameters and χ^2 limits defined in a very restrictive way. The reconstructed track parameters are stored and the associated hits removed from the list corresponding to a given event. The procedure is repeated on the remaining hits with roads and tolerances slightly enlarged. The reconstructed tracks are added to those found previously and the corresponding hits are again removed. The procedure is repeated as many times as specified by the user requirements.

Hits belonging to reconstructed tracks need to be removed from the list of available hits in order to avoid double counting. However, sometimes a given track may have one or several hits in common with another one reconstructed previously. A more sophisticated procedure is thus needed to keep the possibility of reconstructing

crossing tracks. Hits associated to a track already reconstructed can be removed either from the two segments which have been bridged to form this track or only from one of them. In practice, only hits belonging to the second telescope, where tracks are in general more separated, are removed systematically after every iteration. In the upstream telescope, hits belonging to reconstructed tracks are kept in the first iterations. The number of such iterations can be specified by the user.

As mentioned in Section 4.1, two different orderings of the loops on reference planes can be used for the search of track segments in the upstream telescope. One of them was found to be more efficient for low momentum tracks, the other one for high momentum tracks, an effect which can be understood as a consequence of the use of detectors differing very much in size, such as the tiny scintillating fibers and the large drift chambers. The highest global efficiency is reached by the alternate use of the two procedures in successive iterations.

The search for track segments in both telescopes can also be restricted to a given set of detectors. This results in a simpler and less CPU demanding procedure and was also found to enhance the global reconstruction efficiency. The use of a restricted setup is considered as a final step to be performed after the normal reconstruction where all detectors are used. For the LAS configuration, the optimal selection of detectors in the last four iterations was found to be: MMs with STs, DCs with STs, MMs with GMs, and finally MMs and FIs with GMs and FIs.

At the end of the procedure, the fringe field reconstruction is attempted on the remaining hits from the first telescope. This procedure is also iterated as long as new tracks are found in consecutive iterations.

As expected, the iterative procedure increases the computation time compared to a standard, non-iterated reconstruction with the same algorithm. The increase of CPU time has thus to be balanced with the gain in reconstruction efficiency. The plot of efficiency and CPU time (normalized to a non-iterated reconstruction) versus number of iterations is presented in Fig. 10. The calculations were performed on a PC with 600 MHz Pentium III processor running under Linux. The non-iterated reconstruction takes about 170–200 ms/event. The use of seven iterations on full setup is found to be excessively time consuming and therefore the number of iterations is fixed to three on the full setup and four on specified sets of

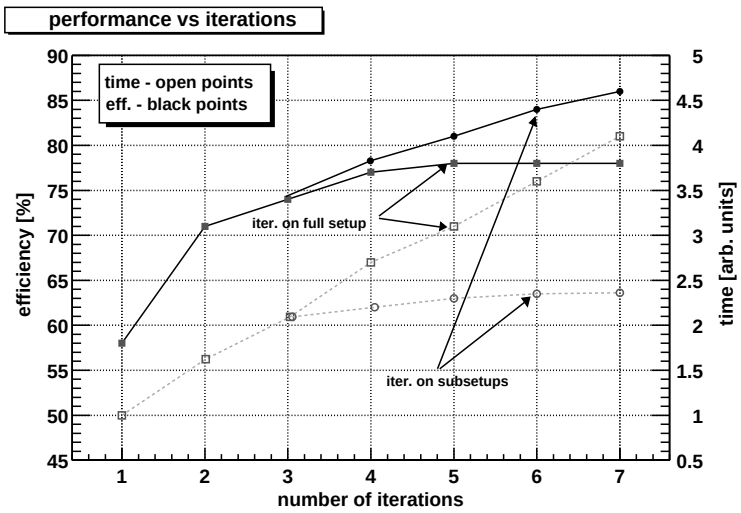

Fig. 10. Reconstruction efficiency and calculation time for different iterations. The black points show the average efficiency for different numbers of iterations. The open points show the corresponding CPU time (in arbitrary units). The squares are related to the full setup, the circles to specified subsets of detectors. The fringe field reconstruction is not included in this plot.

detectors. This choice is optimal for reconstruction time and efficiency. The CPU time increases by a factor of 2.4 as compared to the non-iterated reconstruction.

The reconstruction procedure is controlled by a set of adjustable parameters. General steering parameters define the total number of iterations and the number of iterations before used hits are removed in the upstream telescope. The other parameters can be divided into two groups: the first one defines roadwidth and χ^2 cuts for the reconstruction of segments before and behind the magnet, the second one defines association parameters (cuts for slope and position at the center of SM1) and the χ^2 cut for the spline fit. The actual values of these parameters depend on the iteration number. Their optimal ranges, used in the tests discussed below, are listed in Table 2.

The roadwidths used for target pointing account for the residual curvature of low momentum tracks and for the complexity of the SM1 field map. In the second telescope, target pointing in the non-bending plane requires wider roads due to the longer lever arm. A larger number of additional planes is required in the first iterations when hit combinatorics is large. Fewer planes are required in further iterations, in order to account for less favoured combinations of detectors. The association cuts on y and $\mathrm{d}y/\mathrm{d}z$ have been tuned to avoid the waste of CPU time in useless fits. The high χ^2 limit in the spline fit used in the last iteration reflects the approximate evaluation of multiple Coulomb scattering effects and is mainly needed for low momentum tracks. It has been checked that the fraction of faked tracks does not increase dramatically at the highest allowed values of χ^2.

Table 2
List of adjustable reconstruction parameters[a]

General parameters		
Number of iterations		7
Hits removed from tel. 1 after iter. number		3
Segment search parameters		
	Telescope 1	Telescope 2
Roadwidth in bending pl.	0.1–1.0 mm	(unused)
Roadwidth in non bending pl.	0.1–1.0 mm	1.0–10 mm
Roadwidth in θ pl.	1.0 mm	3.0 mm
Min. no. of additional planes	4–8	5–11
Min. no. θ planes	3–6	2–3
Max. χ^2 segment fit	65	65
Association and track fit parameters		
Association cut on $\mathrm{d}y/\mathrm{d}z$		0.08–0.24
Association cut on y (median plane)		30.0–180 mm
χ^2 cut in spline fit		2–20
χ^2 cut in spline fit for fringe field		20

[a] The quoted ranges correspond to different iterations or detector subsets.

6. Tests on simulated events

The validity of the algorithm described in the previous sections has been tested on simulated data at the two incident momenta foreseen in the COMPASS experiment (100 and 190 GeV). Heavy flavor events at $Q^2 \simeq 0$ have been generated by AROMA [3] and tracked through the COMPASS spectrometer using GEANT [10]. Secondary interactions and other backgrounds, including beam halo, have been fully taken into account and the resulting hits added to those from genuine tracks. The effect of digitization was taken into account according to the characteristics of each detector and detector efficiencies were varied from 100% to 95%. Deep inelastic events at $Q^2 \geqslant 0.5\ \mathrm{GeV}^2$ generated by the Monte-Carlo generator LEPTO [11] were processed in the same way and tested for comparison.

We present here results for AROMA events at 100 GeV satisfying the COMPASS trigger conditions which correspond to selections on Q^2, on the fraction of momentum $1-y$ transferred to the scattered muon and on its azimuthal angle ϕ.

Fig. 11 shows the distribution of the generated momentum for the tracks which are within the detector acceptance and for those which are successfully reconstructed. The contribution of tracks rescued by the reconstruction in the SM1 fringe field amounts to about 25% of the full sample for $p \leqslant 1.5$ GeV.

The distributions of the reconstructed momenta for correct tracks and for faked tracks are compared in Fig. 12. The fraction of faked tracks amounts globally to 10%. Nearly half of it is due to the selection of mirror hits in drift detectors.

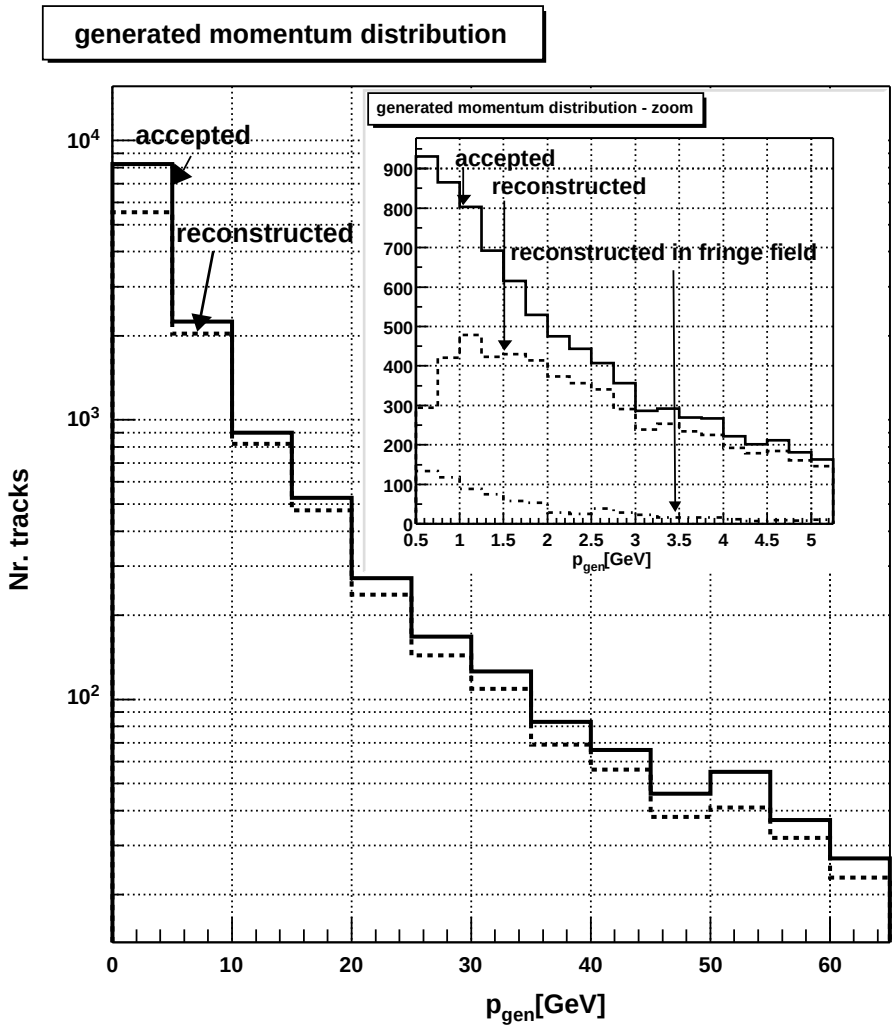

Fig. 11. Distribution of the generated momentum for tracks within the detector acceptance and for reconstructed tracks. The insert shows in addition the distribution for tracks reconstructed in the fringe field of SM1.

When the track parameters are known, the left–right ambiguity solving becomes more efficient. Therefore, some of the faked tracks can be removed by applying this procedure again and redoing the fit. For tracks reconstructed in the fringe field the fraction of faked tracks reaches 27% because wrong hits are often picked up due to the lack of geometrical constraints.

The track reconstruction efficiency (Fig. 13) is fairly constant ($\simeq 85\%$) for momenta above 2.5 GeV and drops to 60% at 1 GeV. We have checked the effect of chamber efficiencies on the reconstruction by introducing an inefficiency of 5% in every detector plane. This results in a drop of 8% in the reconstruction efficiency.

The reconstruction efficiency has also been evaluated for different inputs. When the LEPTO generator is used (also at 100 GeV), we obtain a reconstruction efficiency which is a few percent higher at momenta below 5 GeV and practically unchanged at higher momenta. This effect clearly results from the lower track multiplicity in LEPTO

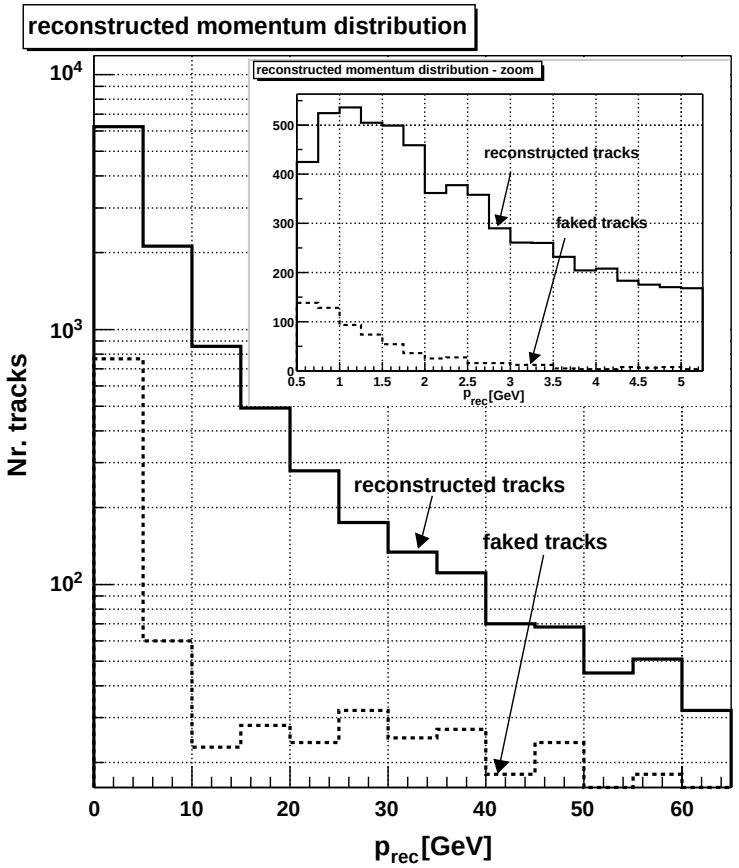

Fig. 12. Distribution of the momentum obtained for all reconstructed tracks and for "faked" tracks.

as compared to AROMA. The sensitivity to the chamber efficiency is also found to be slightly smaller with LEPTO.

When the incoming muon energy is increased to 190 GeV and the AROMA generator is used, we observe a drop of about 5–8% in efficiency over the full momentum range. Part of this effect can again be related to the track multiplicity which is about 30% larger than at 100 GeV. In addition, the change of the angular distribution in the lab frame due to the Lorentz boost makes high multiplicity events more difficult to reconstruct.

Finally, we checked the reconstruction efficiency for charmed meson decays. For D^0 decays at the incoming muon momentum of 100 GeV, for which momentum and angular distributions are shown in Fig. 1, we obtain a reconstruction efficiency of 92% for the K and 94% for the π resulting in a D^0 reconstruction probability of 88%. The additional π from the D^* decay has a reconstruction efficiency of 71%, resulting in a D^* reconstruction probability of 65%. The D^0 and D^* reconstruction probabilities are reduced to 71% and 54%, respectively, when the incoming muon energy is increased to 190 GeV.

7. Conclusions

We have developed and tested a track finding algorithm for the COMPASS large angle spectrometer. The procedure is shown to work with an acceptable efficiency for momenta as low as 0.5 GeV in the difficult context of the COMPASS

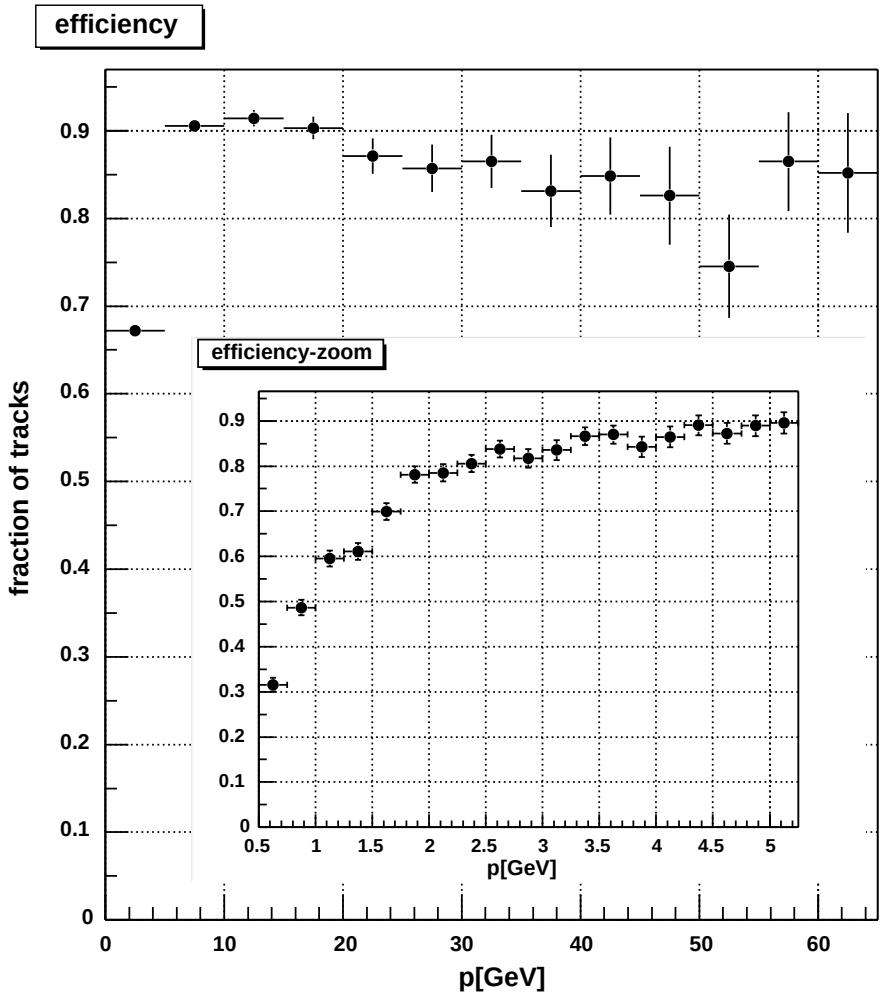

Fig. 13. The track reconstruction efficiency as a function of generated momentum. The insert is a blow-up for low momenta. The events are D^0 events generated by AROMA at incoming momentum of 100 GeV and satisfying the COMPASS trigger requirements.

muon setup where the solenoid target field and the large angle dipole field strongly overlap. As a pattern recognition tool it is fully integrated in the COMPASS reconstruction software where the results are further used for complete track and vertex fits.

Acknowledgements

We wish to thank our colleagues from the COMPASS software group for many constructive remarks and discussions during the development of this project. We are specially grateful to V. Alexakhine, S. Gerassimov, B. Gobbo, M. Lamanna, J.M. Legoff and A. Zvyagin for their advice and assistance at various stages of this work.

References

[1] G.K. Mallot, Spin Physics with COMPASS, Proceedings of the 12th International Symposium on High Energy Spin Physics, Amsterdam 1996, pp. 441–445;

E.M. Kabuss, Nucl. Phys. B (Proc. Suppl.) 79 (1999) 594; L. Schmitt, The COMPASS experiment: Charm physics with muon and hadron beam, presented at the conference on Heavy Quarks at Fixed Target, Rio de Janeiro, October 9–19, 2000, Frascati Physics Series, to be published.

[2] A. Abragam, M. Goldman, Rep. Prog. Phys. 41 (1978) 395.

[3] G. Ingelman, et al., AROMA 2.2, Comput. Phys. Commun. 101 (1997) 135.

[4] The COMPASS Collaboration, COMPASS Proposal, CERN/SPSLC 96-14, SPSC/P297, 1996.

[5] Y. Giomataris, et al., Nucl. Instr. and Meth. A 376 (1996) 29; Ph. Abbon, et al., Nucl. Instr. and Meth. A 461 (2001) 29; D. Thers, et al., Nucl. Instr. and Meth. A 469 (2001) 133.

[6] F. Sauli, et al., Nucl. Instr. and Meth. A 386 (1997) 531; F. Sauli, Nucl. Instr. and Meth. A 419 (1998) 189; S. Bachmann, et al., Nucl. Instr. and Meth. A 461 (2001) 42.

[7] G. Baum, et al., Nucl. Instr. and Meth. A 433 (1999) 207.

[8] H. Wind, Nucl. Instr. and Meth. 115 (1974) 431.

[9] H. Pereira, Ph.D. Thesis, Université de Paris-Sud, Orsay, unpublished.

[10] Cern program library. The version used for the COMPASS experiment can be found at http://wwwcompass.cern.ch

[11] G. Ingelman, et al., LEPTO 6.5, Comput. Phys. Commun. 101 (1997) 108.